Coherency-based Coordination Scheme to Mitigate Adverse Dynamic Interaction of Grid-Forming Inverters

Amirhosein Gohari¹, Muhammad Farooq Umar¹, Mohammad B. Shadmand¹

¹Dept. of Electrical & Computer Engineering, University of Illinois at Chicago, IL, USA agohar2@uic.edu; mumar6@uic.edu; shadmand@uic.edu

Abstract— Due to the better frequency response and transient stability, grid-forming inverters (GFMIs) have shown themselves as a promising solution for the future grid with high penetration of power electronic converters. However, in a network composed of multiple GFMIs using virtual synchronous generator (VSG) as the primary controller, the disturbance from pulse loads or plugin loads may introduce undesired frequency and active power dynamics and oscillations. These adverse dynamics can increase the rate of change of frequency (ROCOF) in some of the buses and disturb transient stability. In this paper, a coherency-based coordination scheme is proposed to eliminate these adverse frequency dynamics and improve frequency nadir in a network comprising fleet of VSG-based GFMIs. The proposed coherencybased coordination selects a coordinative frequency trajectory using the VSG control loop. The proposed coordinative scheme then calculates coordinative coefficients based on which the VSGs start to inject power while maintaining a coherent dynamic response and mitigating adverse dynamic interactions and oscillations. Simulation results for different values of load change in multiple buses are presented to validate the effectiveness of the proposed coordination scheme.

Keywords— Grid-forming inverters, virtual synchronous generator, model predictive control, grid-forming inverters interaction

I. INTRODUCTION

The future power system is shifting from centralized generation to incorporate more distributed generation (DG) i.e., inverter-based DG. This transition in the existing power grid is happening to integrate progressively renewable energy generation sources such as solar-PV, wind energy, etc. In conventional power grid, synchronous generator (SG) is majorly responsible for providing enough system inertia to maintain the transient stability of power system during a sudden contingency such as loss of generation or addition of load [1]. The system inertia is defined as the ability of the power system to resist the changes in the system's frequency because of the kinetic energy stored in the rotating masses such as SGs [2]. However, as inverter based DGs are replacing the SGs in future power grid, the existing power grid is losing its required rotating inertia to maintain the system frequency during the sudden contingencies. The initial rate of change of frequency (ROCOF) during the sudden load change or a generation loss is keep on getting steeper in the future power grid [3, 4]. Thus, the role of providing ample system inertia that can support the system's frequency in transients is much needed from the inverter based DGs.

Conventionally, the inverters were controlled to remain in synchronization with the grid and inject the dictated active and reactive powers. This type of inverter control is known as gridfollowing [5]. However, due to ever increasing requirement of resilient grid operation that are evolved from the high penetration of renewable energy, another inverter control scheme is advanced in last decade that is known as grid-forming inverter (GFMI) control [6]. The GFMI control offers various benefits such as islanded operation and grid connected operation [7], voltage and frequency support, virtual inertia emulation, etc. [8-10]. Moreover, several control schemes of GFMI reported in literature that exhibit great potential to take the role of maintaining transient stability of future power system via inertia emulation [11], fast frequency, and voltage restoration schemes [12, 13]. In [14], a low pass filter is interfaced with a droop control to emulate the virtual inertia and damping via GFMIs. However, with this scheme, the inertia and damping constant are not accessible directly and can't be tunned independently. Another control scheme proposes the lead-lag filter-based droop control for GFMIs to incorporate more direct tunning of inertia and damping constant [15]. But the lead-lag filter-based GFMI control is not able closely mimic the SG's dynamic behavior. Thus, a promising solution to emulate virtual inertia and dynamics of SGs for frequency support via GFMI is to leverage virtual synchronous generator (VSG) based control scheme [16]. In this type of control, the swing equation of SG is leveraged to generate the voltage references to control the GFMIs. This gives more direct access to characteristic parameters of SG such as inertia coefficient and damping constant which enables the GFMIs to closely mimic the dynamic and steady-state behavior of SG and compensate for the decreased rotating inertia and improving the transient stability of the future power grid.

Although the VSG based GFMIs improves the transient stability, but it introduces oscillations in active power and frequency prominently under multi-VSG based grid in response to severe transients. Addressing this issue in multi-VSG based grid is not covered comprehensively in the existing literature. In fact, due to low inertia of upcoming power grids dominated by inverter-based DGs, the grid disturbances will have more severe impact on the frequency in comparison to the traditional power system [17-19]. Such frequency oscillations, after load addition or loss of generation can have catastrophic impact on operation of entire network and may result in cascaded tripping of nearby interconnected inverters. In [20], a small signal model of VSG based GFMI is developed. Moreover, the damping constant and inertia constant of the VSG control is adjusted to suppress these

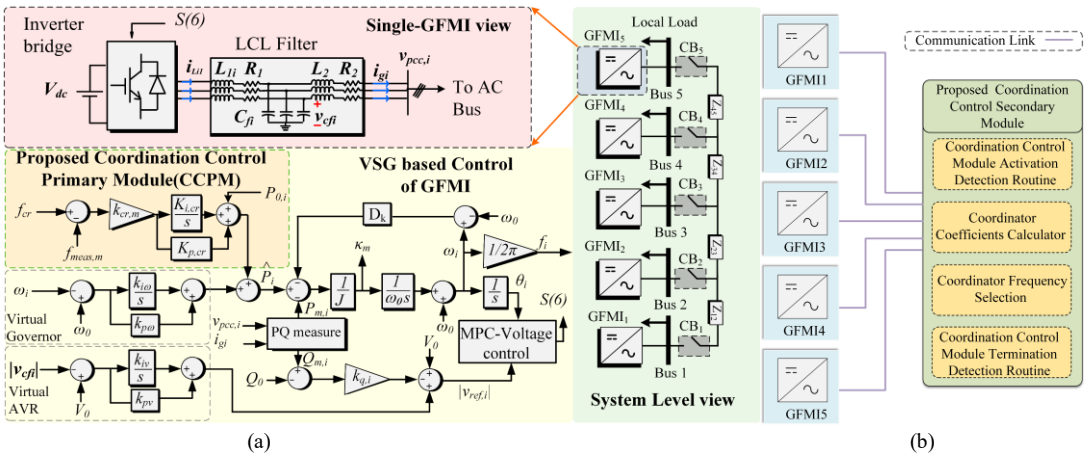


Fig.1. Understudy system with structure of proposed coordination control and VSG based GFMI control (a) the primary controller with the proposed coordination control primary module, single GFMI, and the topology of the grid (b) The topology of the communication line between the coordination control and the inverters and the components of the coordination control module.

oscillations in the frequency and fluctuations in active power. The presented analysis doesn't include the effect of multi-VSG and the impact from the neighboring GFMIs during a disturbance. An adaptive virtual inertia and customized damping constant based scheme is proposed in [21] to improve the transient stability of the system during the frequency excursions. However, the devised adaptive inertia and damping constants doesn't represent the optimal values of inertia and damping constants and the impact of the line impedances in the interconnected network is also ignored. The work in [22], proposed an active power and frequency based admittance model to analyze the small signal stability. This model encompasses the network parameters in the developed model. Moreover, an output admittance model is presented in [23] that involves in developing the transfer functions of the multi-VSG network considering the line impedances between them. The origin of oscillations in frequency and active power of multi-VSG network is discussed. However, still in the previous literature the solution to the oscillations in frequency and active power of multi-VSG network of GFMIs considering the network dynamics and line impedance is missing.

This paper proposes a coordination scheme to mitigate the adverse dynamics of the frequency and active power in a network dominated by VSG-based GFMIs. According to the effect of load variation and generation disturbances on the frequency, the proposed coherency-based coordination control scheme will be triggered. The triggering mechanism is based on the frequency trajectory of each VSG obtained from their control loop. Once the coherency-based coordination control scheme is triggered, it determines a coordinator frequency as an enforcing reference point for VSGs' frequency dynamic. Then, the proposed scheme injects the coordinator power in the nominal active power reference of VSGs to mitigate adverse frequency and active power oscillations during transient. Furthermore, the frequency of the VSGs acts more coherent during the transients, which makes the frequency nadir of all the VSGs closer to each other and hence, mitigating the adverse interactions in multi-VSG based GFMIs. The section II of the paper the discuss the VSG based primary controller development. The mechanism and development of proposed coherency-based coordination approach is presented in the section III. Section IV presents the simulation results to prove the effectiveness of the proposed approach. Finally, the conclusion and future work is presented in the section V of the paper.

II. OVERVIEW OF GFMI'S PRIMARY CONTROL METHOD

Fig.1 illustrates the structure of single GFMI interfaced with LCL filter and its primary controller. In normal condition, the proposed coordination control primary module is transparent. In this situation, the frequency-active power (f-p) control loop of the GFMI is expressed via emulation of the swing equation. Moreover, the voltage magnitude-reactive power (v-Q) dynamics of the GFMI are based on the droop-based control. Thus, the generation of the voltage reference for the VSG based GFMI is given by,

$$J_{i}\omega_{0}\frac{d(\omega_{i}-\omega_{0})}{dt} = \hat{P}_{i} - P_{m,i} - D_{k,i}(\omega_{i}-\omega_{0})$$

$$\hat{P}_{i} = (k_{p\omega} + \frac{k_{i\omega}}{s})(\omega_{0}-\omega_{i}) + P_{0,i}$$

$$\theta_{i} = \int \omega_{i} dt$$
(1)

$$|v_{ref,i}| = -k_{q,i}(Q_{m,i} - Q_{0,i}) + (k_{pv} + \frac{k_{iv}}{s})(V_0 - |v_{cfi}|) + V_0$$
 (2)

where i is the index number for GFMIs, J_i is inertia constant for i^{th} GFMI, $P_{0,i}$ and $P_{m,i}$ are the nominal and measured active powers, ω_i and ω_0 are the measured angular frequency and nominal angular frequency, $D_{k,i}$ is the damping coefficient, and θ_i refers to the voltage angle. Meanwhile, $k_{p\omega}$ and $k_{i\omega}$ are the proportional and integral gain of the virtual governor. $Q_{0,i}$ and $Q_{m,i}$ are the nominal and measured reactive powers, V_o is the nominal magnitude of the output voltage, and $k_{q,i}$ refers to the v-Q droop gain. Furthermore, k_{pv} and k_{iv} are the proportional and integral gain of the virtual AVR, and $|v_{ref,i}|$ the magnitude of the reference voltage. The voltage reference generated via (2) is regulated via model predictive control (MPC). The MPC control scheme is chosen over the conventional PI based control to incorporate the inherent advantages of MPC such as low/no tunning effort, no nested/double loops, and faster dynamic response [24, 25].

The MPC involves deriving and discretizing the state-space model for the inverter interfaced with LCL filter as depicted in the Fig.1. The continuous-time state-space model for the LCL filter is given by,

$$\frac{d}{dt} \begin{bmatrix} i_{Li1} \\ v_{cfi} \\ i_{gi} \end{bmatrix} = A \begin{bmatrix} i_{Li1} \\ v_{cfi} \\ i_{gi} \end{bmatrix} + B [v_{bri}] + D [v_{pcc,i}]$$
(3)

where, i defines the index number for the GFMIs, i_{Lil} is the inverter-side current, i_{gi} is denoted as the output current, v_{cfi} is the capacitor voltage, v_{bri} is the inverter's bridge voltage, and v_{pcci} is the point of common coupling voltage. The continuous-time A, B, and D matrices are defined as

$$A_{i} = \begin{pmatrix} -\frac{R_{i1}}{L_{i1}} & -\frac{1}{L_{i1}} & 0\\ \frac{1}{C_{fi}} & 0 & -\frac{1}{C_{fi}}\\ 0 & \frac{1}{L_{i2}} & -\frac{R_{i2}}{L_{i2}} \end{pmatrix}, B_{i} = \begin{pmatrix} 1/L_{i1}\\ 0\\ 0 \end{pmatrix} \text{ and } D_{i} = \begin{pmatrix} 0\\ 0\\ -\frac{1}{L_{i2}} \end{pmatrix}$$

where, R_{il} , R_{i2} , L_{il} , L_{i2} , and C_{fi} are the values of the *LCL* filter's passive elements. The discretized form of the (3) in $\alpha\beta$ frame reveals the one step ahead predicted values of the state variables and it is given by,

$$\begin{bmatrix} i_{Li1,k+1}^{\alpha} \\ v_{cfi,k+1}^{\alpha} \\ i_{gi,k+1}^{\alpha} \end{bmatrix} = A_{id} \begin{bmatrix} i_{Li1,k}^{\alpha} \\ v_{cfi,k}^{\alpha} \\ i_{gi,k}^{\alpha} \end{bmatrix} + B_{id} \begin{bmatrix} v_{bri,k}^{\alpha} \end{bmatrix} + D_{id} \begin{bmatrix} v_{pcci,k}^{\alpha} \end{bmatrix}$$

$$\begin{bmatrix} i_{Li1,k+1}^{\beta} \\ v_{cfi,k+1}^{\beta} \\ i_{gi,k+1}^{\beta} \end{bmatrix} = A_{id} \begin{bmatrix} i_{Li1,k}^{\beta} \\ v_{cfi,k}^{\beta} \\ i_{gi,k}^{\beta} \end{bmatrix} + B_{id} \begin{bmatrix} v_{bri,k}^{\beta} \end{bmatrix} + D_{id} \begin{bmatrix} v_{pcci,k}^{\beta} \end{bmatrix}$$

$$(4)$$

where α and β superscript show the corresponding alpha and beta component of a variable in $\alpha\beta$ frame. The discretized forms of system matrix A_d , input matrix B_d , and feedforward matrix D_d are obtained by,

$$A_{id} = e^{A_i T_s}, \ B_{id} = \int_0^{T_s} e^{A_i \tau} d\tau B_i = \left[\frac{e^{A_i \tau}}{A_i} \right]_0^{T_s} B_{id} = A_i^{-1} (A_{id} - I) B_i,$$

$$D_{id} = A_i^{-1} (A_{id} - I) B_i$$

Hence, based on the system model presented by (4), the cost function is generated by calculating the magnitude of subtraction of $\vec{v}_{ref,\alpha\beta}$ generated via proposed VSG based control loop and possible output voltage $\vec{v}_{cfi,\alpha\beta}$, which can be show as follows,

$$g = |\vec{v}_{ref}^{a\beta} - \vec{v}_{cfi,k+1}^{a\beta}|$$

$$\vec{v}_{cfi,k+1}^{a\beta} = v_{cfi,k+1}^{a} + jv_{cfi,k+1}^{\beta}$$

$$S_{k+1} = \arg\min(g)$$
(5)

Three-phase GFMI has 8 switching vectors (S_k) and for each switching vector the cost function in (5) is calculated and compared with the previous value. The switching vector that represents lowest value of cost function is selected as an optimized vector and switching sequence related to that

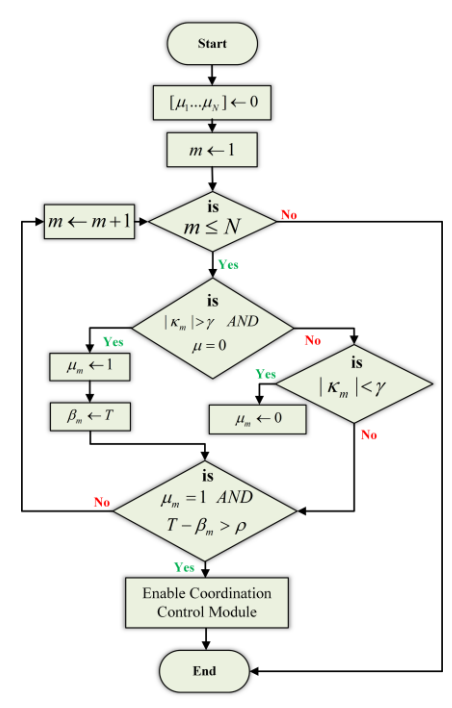


Fig. 2 Activation Detection Routine in the proposed coordination control secondary module flowchart.

switching vector is selected as output of MPC to regulate the PCC voltage according to reference generated.

III. THE PROPOSED COHERENCY-BASED COORDINATION SCHEME

The proposed coherency-based coordination schemes mitigate the adverse dynamics between the GFMIs by changing the nominal power of the VSGs after a load change. The block diagram of the coordination control primary module can be seen in Fig. 1(a). The coordination module needs communication links which transfer frequencies, f_{ν} , and frequency trajectories, κ_m of the VSG control loop to the coordination control secondary module, which is illustrated in Fig. 1(a). The coordination control secondary module has four components, i.e., coordination control activation routine, coordinator coefficient calculator, coordinator frequency selection, and coordination control termination detection routine. The activation detection routine decides about the start of the corrective action of the coordination control and activates the primary control modules inside each VSG in the grid. Before the activation of the coordination control, the coordination control primary module is transparent. The flowchart of the activation routine is shown in Fig. 2. In this flowchart, T shows the current time of the system, and β_m and μ_m are the local variables used by the detection algorithm to store data corresponds to the m^{th} VSG in the grid. Furthermore, N is the total number of VSGs in the grid. The activation detection routine starts by initializing the vector of all the μ to zero. Then, it checks κ_m , which is obtained from the control loop of m^{th} VSG as shown in Fig.1(a). If the value of κ_m surpasses the predefined value γ for the predefined time span ρ the coordination control is enabled. When κ_m goes beyond the predefined value, μ_m becomes one and β_m stores the current time of the system. After the coordination control starts its corrective action, the coordinator coefficients calculator inside the

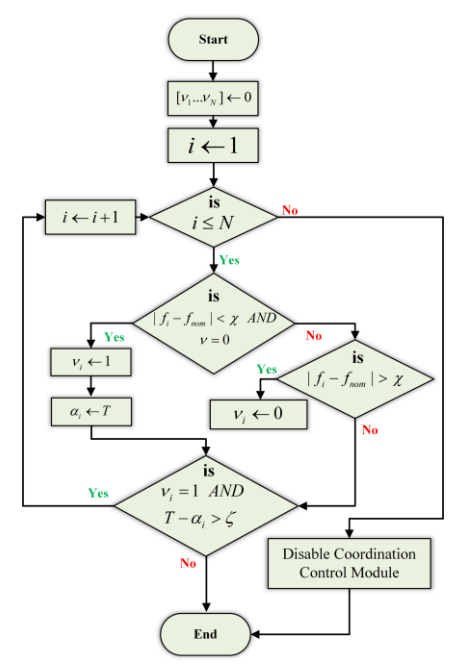


Fig. 3 Termination detection algorithm in the proposed coordination control secondary module.

coordination control secondary module, calculates the coordinator coefficient K_{cr} for all the VSGs in the grid. To calculate coordinator coefficients for the VSGs, based on the maximum of frequency trajectories obtained from the control loop of the VSG, the parameter λ is calculated as follows,

$$\lambda = \max \{K\}$$

$$K = [\kappa_m], 1 \le m \le N$$
(6)

where κ_m is obtained from the control loop of m^{th} VSG and N is the total number of GFMIs in the considered network. The coordinator coefficient $K_{cr,m}$ for the m^{th} VSG in the grid is calculated from the following relation,

$$K_{cr,m} = \frac{K_m}{\phi} \tag{7}$$

where ϕ is obtained from the following relation,

$$\phi = \min\{K\} \tag{8}$$

The next step is to determine the coordinator frequency as an enforcing reference point for VSGs' frequency dynamic. This coordinator frequency is determined based on minimum frequency trajectories calculated in (9). Then, the frequency of the VSG that has minimum frequency trajectory will be selected as the coordinator frequency, f_{cr} . After the coordinative frequency f_{cr} is determined, a coordinative power is injected to the nominal power of the VSGs to make the frequencies coherent during transients. The coordinative power for m^{th} GFMI can be calculated as follows,

$$P_{cr,m} = (f_{cr} - f_{meas,m}) K_{cr,m} (K_{p,cr} + \frac{K_{i,cr}}{s})$$
 (9)

where $f_{meas,m}$ is the measured frequency in the m^{th} GFMI in the network, $K_{p,cr}$ and $K_{i,cr}$ are PI coefficient for the coordinative power, $K_{cr,m}$ is the coordinator coefficient of m^{th} VSG in the grid

Table I: SYSTEM SPECIFICATION

Parameter	Value
Rated Power of the VSGs connected to bus #1 and bus #3	10 kW
Rated Power of the VSGs connected to bus #2, #4, and #5	12kW
Rated Phase Voltage	120V
L_{inv}	1.8 mH
L_{g}	0.45 mH
C_f	43 μF
J	0.05 kgm2
Damping Coefficient of the VSGs connected to bus #1 and bus #3	265
Damping Coefficient of the VSGs connected to bus #2, #4, and #5	318
$Z_{12,} Z_{23,} \ Z_{34,} Z_{45}$	0.805 + j4.33, 0.49 + j2.63, 0.4305 + j2.31, 0.56 + j3.01

TABLE II: VALUE OF LOADS

Bus Number	Active load (kW)	Reactive load (kVAR)
1	7.56	3.66
2	6.61	6.56
3	5.79	4.95
4	8.71	5.85
5	4.65	5.01

which is defined after the determination of φ and f_{cr} by the coordination system.

The coordinative power is added to the nominal power of the VSGs to mitigate their adverse frequency and power dynamics until the termination of the coordination module if detected by the termination detection routine. The flowchart of the termination detection routine is shown in Fig. 3. In this flowchart, α_i represents the time at which the i^{th} VSG's frequency is in the acceptable boundary, specified by χ . Furthermore, v_i become one when the i^{th} VSGs frequency goes into the acceptable boundary and becomes zero when the frequency goes out of the acceptable boundary. T denotes the current time of the system. The termination detection algorithm starts by making all the elements of the v vector zero. Then, a loop starts with loop variable i that calculates the absolute value of the difference between the frequency of each VSG in the grid and the nominal frequency. Then, this difference is compared with the predefined value χ . If the absolute difference between all the VSGs' frequency and nominal frequency remains less than χ for predefined time span of ξ the coordination control scheme is terminated. After the coordination control is terminated, the coordination control primary module become transparent, and the system returns to its normal operation.

IV. RESULTS AND DISCUSSION

The effectiveness of the proposed scheme is validated in a radial network whose generation units are all VSG-based GFMI. Table I lists the parameters of the VSG and the related line impedances between each VSG. Table II shows the values of the nominal loads. The values of the $K_{p,cr}$ and $K_{i,cr}$ gains of the coordinative control are tunned and selected as 400 and 20, respectively. The value of γ and ρ are 20 and 1.7ms in the

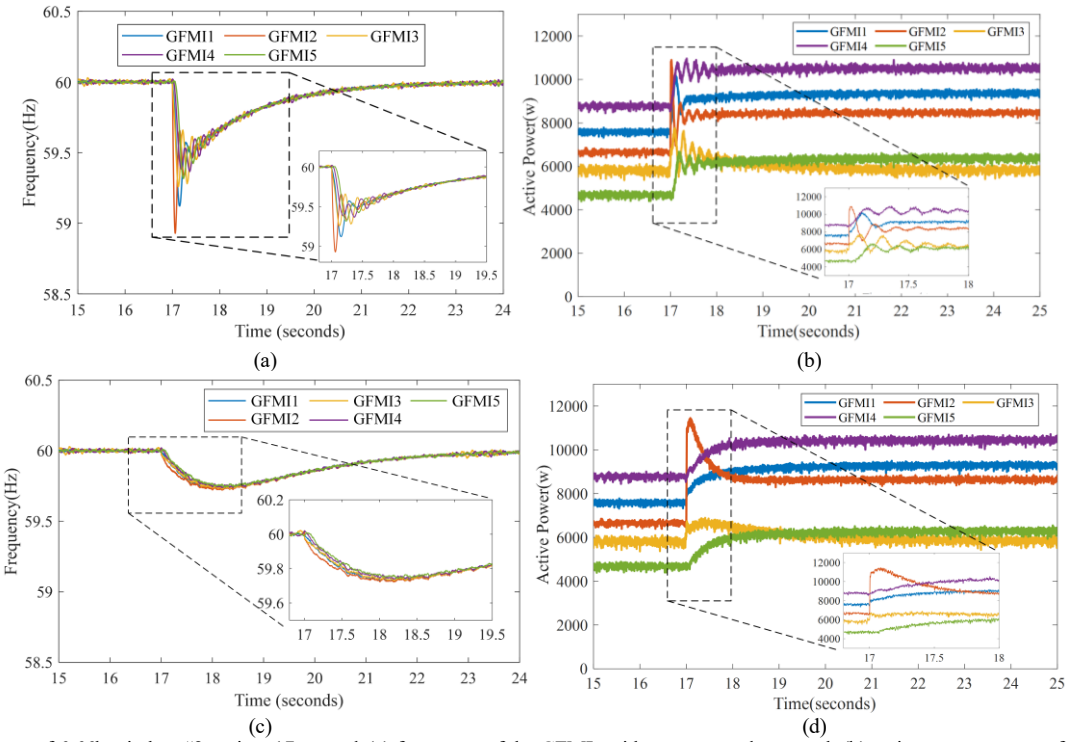


Fig. 4. load increase of 6.66kw in bus #2 at time 17 seconds(a) frequency of the GFMIs without proposed approach (b) active output power of all the GFMIs in the grid without proposed approach (c) frequency of the GFMIs with proposed approach (d) active output power of all the GFMIs in the grid with proposed approach

activation detection routine, respectively. Moreover, χ and ξ are 0.05 and 0.5s in termination detection algorithm, respectively. For the validation of the proposed method, the VSG-based GFMIs are studied for the dynamic response during the load disturbance at different nodes of the considered network. Moreover, the results are compared without adding the proposed coordination scheme.

A. Case A: 6.6 kW load addition on Bus # 2

This case study refers to the addition of a 6.6 kW load at Bus #2 at time 17 seconds. Fig. 4 (a) shows the frequency transient response of all the GFMIs to the load addition without using the proposed coordination scheme. Specifically, the VSGs suffer from the frequency oscillations that can be lethal for the resilient operation of the power system. More oscillations and lower frequency nadir are observed in the frequency dynamic response of GFMI₂ because of its position with respect to bus #2 that experienced load change in the grid. On the other hand, for the GFMI₅, the frequency deviation is less than the other GFMIs. Fig. 4 (b) illustrates the active power profiles of the GFMIs without the proposed control during the load disturbance. Similarly, the oscillations in the active power output of GFMI are also observed in their active powers which can disrupt the transient stability of the system. In contrast, when the proposed coordination scheme is applied, the frequency dynamic response is improved. Fig. 4 (c) and Fig. 4 (d) depict the frequency and the active power output of all the GFMIs after implementation of the proposed control scheme. After 2.26 seconds, the load change is detected by activation detection routine, and the primary coordination control module in each VSG start to manipulate nominal power of VSGs to mitigate the adverse dynamics of frequency and active power. As can be seen from Fig. 4(c) and Fig. 4(d) and zoomed in window of the plots, the frequency and active power oscillation considerably decreased by using the proposed coordination scheme. Along with mitigating adverse dynamic of active power and frequency, the proposed coordination scheme can improve frequency nadir in all the buses. After applying coordinator power to mitigate adverse dynamics, at 22.502 seconds, the termination detection module, deactivates the primary coordination module.

B. Case B: 5 kW load increase on bus # 5

In this case study, the location where the load is added is changed to bus # 4. This case study is preformed to validate the correct functionality of the proposed coordination control when load change happens in another bus of the grid. Based on the load change information the proposed control autonomously adjusts the parameters of the controller to effectively mitigate the oscillations in the frequency and active power output of the GFMIs. Fig. 5 (a) and Fig. 5 (b) illustrate the dynamic response of frequency and active power for all GFMIs due to the 5kW load change at bus # 5 without the proposed scheme. As shown in these figures, the frequency and active power of the GFMIs have significant oscillations. The frequency nadir of the GFMI connected to bus #4 is less than the other GFMIs in the grid. Fig. 5(c) and Fig. 5(d) show frequency dynamics and active power of the GFMIs in the grid with the proposed coordination control. After 2.46ms the activation detection routine triggers the primary coordination control module inside the GFMIs and they start to add coordinator power to GFMIs nominal power. As

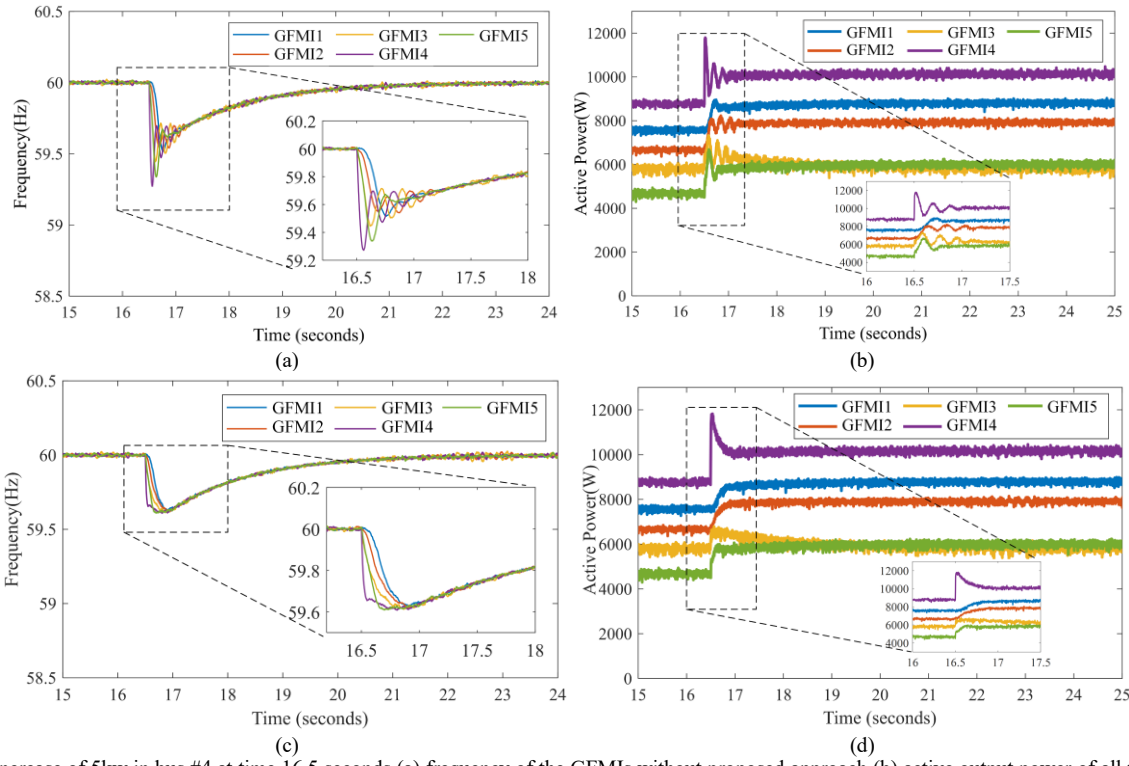


Fig. 5. load increase of 5kw in bus #4 at time 16.5 seconds (a) frequency of the GFMIs without proposed approach (b) active output power of all the GFMIs in the grid without proposed approach (c) frequency of the GFMIs with proposed approach (d) active output power of all the GFMIs in the grid with proposed coordination scheme

shown in Fig. 5(c) and fig. 5(d) the frequency and active power oscillation is significantly reduced using the proposed coordination scheme. Along with decreasing the oscillations, the frequency nadir of all the buses in the grid improved by applying the proposed coordination control scheme. The proposed scheme add coordinator power to the VSGs' active power until 22.7s at which the termination detection routine deactivate the primary coordination control module inside the VSGs

V. CONCLUSION

In this paper, a coherency coordination control scheme is proposed to mitigate the adverse dynamics of active power and frequency during the load change. The proposed scheme adds a coordinative power to the VSG nominal power which is implemented using coordination control primary module in each VSG and coordination control secondary module that receives the information of all the frequencies and frequencies trajectories in the VSGs' control loop. The derivation of the coordinator frequency and coordinator coefficients which incorporate in obtaining coordinative power is described in the paper. Furthermore, the algorithms which determine the start and end of the proposed coordination control primary module operation are described in detail in the paper. The validity of the proposed algorithm is tested via the MATLAB/SIMULINK simulation. The simulation results for load changes in the grid with and without the proposed coordination scheme is presented in the paper which shows prominent impact of the proposed scheme in mitigating adverse frequency and active power dynamics during the load change.

ACKNOWLEDGMENT

This work was supported by the U.S. National Science Foundation under Grant ECCS-2114442. The statements made herein are solely the responsibility of the author.

REFERENCES

- [1] X. Xiong, C. Wu, P. Cheng, and F. Blaabjerg, "An Optimal Damping Design of Virtual Synchronous Generators for Transient Stability Enhancement," *IEEE Transactions on Power Electronics*, vol. 36, no. 10, pp. 11026-11030, 2021, doi: 10.1109/TPEL.2021.3074027.
- [2] J. H. Eto, J. Undrill, C. Roberts, P. Mackin, and J. Ellis, "Frequency control requirements for reliable interconnection frequency response," 2018.
- [3] N. I. B. R. P. Task, "Fast frequency response concepts and bulk power system reliability needs," NERC, p. 1, 2020.
- [4] A. Khan, M. Hosseinzadehtaher, M. B. Shadmand, S. Bayhan, and H. Abu-Rub, "On the stability of the power electronicsdominated grid: A new energy paradigm," *IEEE Industrial Electronics Magazine*, vol. 14, no. 4, pp. 65-78, 2020.
- [5] M. F. Umar et al., "Single-Phase Grid-Interactive Inverter with Resonance Suppression based on Adaptive Predictive Control in Weak Grid Condition," *IEEE Journal of Emerging and Selected Topics in Industrial Electronics*, vol. 3, no. 3, pp. 809-820, 2021.
- [6] M. Hosseinzadehtaher, A. Zare, A. Khan, M. F. Umar, S. D'silva, and M. B. Shadmand, "AI-based Technique to Enhance Transient Response and Resiliency of Power Electronic Dominated Grids

- via Grid-Following Inverters," *IEEE Transactions on Industrial Electronics*, 2023.
- [7] B. Nun, M. F. Umar, A. Karaki, M. B. Shadmand, S. Bayhan, and H. Abu-Rub, "Rank-based predictive control for community microgrids with dynamic topology and multiple points of common coupling," *IEEE Journal of Emerging and Selected Topics in Industrial Electronics*, vol. 3, no. 1, pp. 144-155, 2021.
- [8] G. Yuan, "Grid-Forming Technologies Enabling a Decarbonized Power System [Technology Leaders]," *IEEE Electrification Magazine*, vol. 10, no. 1, pp. 7-9, 2022.
- [9] D. B. Rathnayake et al., "Grid forming inverter modeling, control, and applications," *IEEE Access*, vol. 9, pp. 114781-114807, 2021.
- [10] Y. Lin et al., "Research roadmap on grid-forming inverters," National Renewable Energy Lab.(NREL), Golden, CO (United States), 2020.
- [11] A. Zare, S. D'silva, and M. B. Shadmand, "Optimal Ratio of Grid-Forming to Grid-Following Inverters Towards Resilient Power Electronics Dominated Grids," in 2023 IEEE Applied Power Electronics Conference and Exposition (APEC), 2023: IEEE, pp. 2347-2352.
- [12] R. H. Lasseter, Z. Chen, and D. Pattabiraman, "Grid-forming inverters: A critical asset for the power grid," *IEEE Journal of Emerging and Selected Topics in Power Electronics*, vol. 8, no. 2, pp. 925-935, 2019.
- [13] J. L. Rodríguez-Amenedo, S. A. Gómez, M. Zubiaga, P. Izurza, J. Arza, and J. D. Fernández, "Grid-Forming Control of Voltage Source Converters based on the Virtual-Flux Orientation," *IEEE Access*, 2023.
- [14] J. Liu, Y. Miura, and T. Ise, "Comparison of dynamic characteristics between virtual synchronous generator and droop control in inverter-based distributed generators," *IEEE Transactions on Power Electronics*, vol. 31, no. 5, pp. 3600-3611, 2015.
- [15] W. Zhang, A. M. Cantarellas, J. Rocabert, A. Luna, and P. Rodriguez, "Synchronous power controller with flexible droop characteristics for renewable power generation systems," *IEEE Transactions on Sustainable Energy*, vol. 7, no. 4, pp. 1572-1582, 2016.

- [16] M. H. Othman *et al.*, "Progress in control and coordination of energy storage system - based VSG: a review," *IET Renewable Power Generation*, vol. 14, no. 2, pp. 177-187, 2020.
- [17] J. Alipoor, Y. Miura, and T. Ise, "Stability assessment and optimization methods for microgrid with multiple VSG units," *IEEE Transactions on Smart Grid*, vol. 9, no. 2, pp. 1462-1471, 2016.
- [18] M. F. Umar, M. Hosseinzadehtaher, M. B. Shadmand, H. Livani, and M. Ben-Idris, "A Corrective Scheme to Prevent Adverse Dynamic Interaction of Grid-forming Inverters," in 2023 IEEE Power & Energy Society Innovative Smart Grid Technologies Conference (ISGT), 16-19 Jan. 2023 2023, pp. 1-5, doi: 10.1109/ISGT51731.2023.10066342.
- [19] M. F. Umar, M. Hosseinzadehtaher, and M. B. Shadmand, "Enabling Aggregation of Heterogenous Grid-Forming Inverters via Enclaved Homogenization," *IEEE Access*, vol. 10, pp. 94765-94777, 2022, doi: 10.1109/ACCESS.2022.3204340.
- [20] H. Wu *et al.*, "Small-signal modeling and parameters design for virtual synchronous generators," *IEEE Transactions on Industrial Electronics*, vol. 63, no. 7, pp. 4292-4303, 2016.
- [21] D. Li, Q. Zhu, S. Lin, and X. Bian, "A self-adaptive inertia and damping combination control of VSG to support frequency stability," *IEEE Transactions on Energy Conversion*, vol. 32, no. 1, pp. 397-398, 2016.
- [22] P. Zhang, H. Cai, J. Shi, and X. He, "Stability analysis of parallel inverter systems using a P/w (Q/E)"Admittance"," in *Proceedings of the CSEE*, 2016, vol. 36, no. 9, pp. 2486-2493.
- [23] B. Qin, Y. Xu, C. Yuan, and J. Jia, "A unified method of frequency oscillation characteristic analysis for multi-VSG gridconnected system," *IEEE Transactions on Power Delivery*, vol. 37, no. 1, pp. 279-289, 2021.
- [24] J. Rodriguez et al., "State of the Art of Finite Control Set Model Predictive Control in Power Electronics," *IEEE Transactions on Industrial Informatics*, vol. 9, no. 2, pp. 1003-1016, 2013, doi: 10.1109/TII.2012.2221469.
- [25] M. B. Shadmand, S. Jain, and R. S. Balog, "Autotuning Technique for the Cost Function Weight Factors in Model Predictive Control for Power Electronic Interfaces," *IEEE Journal of Emerging and Selected Topics in Power Electronics*, vol. 7, no. 2, pp. 1408-1420, 2019, doi: 10.1109/JESTPE.2018.2849738.